WILEY | Hindawi

Research Article

Urban Arterial Signal Coordination Using Spatial and Temporal Division Methods

Lei Feng [iD],[1] Xin Zhao [iD],[1] Haobo Lin,[2] and Rui Li [iD][1]

[1]*School of Transportation and Logistics Engineering, Wuhan University of Technology, Wuhan 430063, China*
[2]*School of Architecture and Transportation Engineering, Guilin University of Electronic Technology, Guilin 541004, China*

Correspondence should be addressed to Xin Zhao; zhaoxin@whut.edu.cn

Traffic signal coordination on urban arterials often requires that timing plans be divided either spatially into clusters of signalized intersections or temporally as time-of-day-based plans. This research proposes a method of dividing timing plans by both spatial and temporal factors simultaneously, in order to provide a dynamic coordinated signal control plan suitable for handling variations in intersection demands and fluctuations in traffic flow. The optimal coordination phase difference of adjacent space coordination subarea is obtained through the method of set operation, so that the spatial subareas can be connected. Similarly, timing plans are dynamically grouped into times of day using the concept of risk decision-making by solving the minimum value of the risk function. Divisions can be further adjusted in real time by changing the conditions, thus resulting in dynamic coordinated signal control. The proposed method was tested in a microscopic simulation of a real-world arterial based on empirical volumes and turning movements. The results showed that the proposed model produced greater reductions in delay and queue length when compared to the methods that subdivide by spatial or temporal thresholds alone. Sensitivity analysis revealed that the proposed method was better suited to imbalances in directional volumes when compared to spatial or temporal division methods alone.

1. Introduction

As worldwide traffic demand continues to grow, engineers are faced with significant challenges in managing increased urban congestion. A great deal of research has focused on the coordination of traffic signals to allow smooth progression for multiple traffic movements within a network. On arterials, through route progresses via the maintenance of a "band" or "wave" of green signals for the platoons of vehicles traveling in both directions. Since the green wave coordinated control theory was proposed [1, 2], the strategy was expanded to different roadways and conditions. The coordinated control methods for urban arterial roads can usually be divided into two categories: the optimization of green wave bandwidth and the optimization of other measures of effectiveness such as minimum delay time, stops, and queue length. Green wave optimization problems include

numerical solution methods [3–5], graphic solution methods [6, 7], and modeling methods [8–12]. One of the most popular modeling methods is the MAXBAND model [13], a multipath maximum green wave bandwidth model. The MULTIBAND model requires the centerline of the green band to be symmetrical, that is, identical vehicle speeds and bandwidth size in both directions, which greatly limits the bandwidth of the green phase. For this reason, a multi-bandwidth model (AM-Band) with an asymmetric green band centerline is proposed [14]. Although turning movements were not considered in the original AM-Band model, later studies considered non-through traffic [15, 16].

Increasing traffic also produces variable traffic, with dynamic changes in demand throughout the day and season. These traffic characteristics make it difficult to implement green wave coordinated control and to achieve satisfactory coordination effects. Several studies have

investigated the subdivision of progression zones [17] and signal timing plan schedules to better adapt to changing conditions [18–20]. Other studies have considered methods to subdivide control zones specifically for coordinated urban arterials [21]. There has been little research into the coordinating control among subareas at the transition zones, thus limiting the ability to provide a coordinated traffic control along exceptionally long corridors.

In an attempt to manage fluctuations in the temporal and spatial distribution of traffic flow, researchers have developed several methods to subdivide timing plans across multiple times of the day. This approach is favored by most traffic managers for its low operating cost and ease of implementation. Since the hierarchical clustering method was first introduced to the study of multi-period division of traffic control [22], there have been several other studies on multi-period division of signal control timing plans [23, 24]. An improved K-means clustering method was used to divide the daytime partitions. Ma et al. determined the optimal time partition breakpoint through the optimization process [25, 26]. However, these studies have generally focused on isolated intersections rather than multi-signal arterials and coordinated control. In addition, some scholars have also paid attention to the control boundary division of urban road networks. A back pressure-based model was used to optimize the maximum throughput of the road network in oversaturated traffic conditions. Ma et al. [27] proposed a signal optimization method on this basis. Ding et al. established a congested area range estimation model by using the density wave transfer velocity, and then based on the 3D macroscopic fundamental graph surface model, a dynamic boundary sliding mode control method was proposed to assess the entrance of the congested area, so as to determine the control boundary and dynamic changes [28]. The method proposed by Niu et al. is similar to this article [29], which considers both time and space, and a spatiotemporal comprehensive traffic partitioning method is proposed based on clustering. The difference is that they start with vehicle trajectory data to optimize the control subdivision.

The above research expounds the division of urban traffic control boundaries from different scenarios, which has a positive effect on the inspiration of this article. It should be pointed out that in the existing research, little attention has been paid to the problems of coordinated control boundary division and coordinated subarea division of urban arterial corridors. The continuous expansion of urban traffic demand leads to a continuous increase in the length of arterial corridors, and its control difficulty also increases. The strong temporal and spatial variations of traffic arterial corridors make it meaningful to divide the control boundary, and its congestion points and areas will appear in different time and space. Therefore, it is necessary to consider the temporal and spatial influencing factors to optimize the division of urban arterial coordination control subareas. Since there are various traffic modes at the intersection, pedestrians

and non-motor vehicles also participate in traffic activities, and the signal lights are affected by the temporal and spatial changes in traffic, which belongs to the multitransport mode coordinated control optimization problem under the dynamic response mechanism.

In summary, the existing research on traffic signal coordination has focused on subdividing either by time (e.g., time-of-day plans) or space (e.g., coordination zones). However, this approach has shortcomings when applied to a highly variable traffic flow that exhibits inconsistent patterns both by time and area. For example, a space-based approach can only adapt to the change in time dimension by continuously adjusting the subdivision of the spatial dimension. Similarly, a time-based subdivision method may attempt to categorize traffic periods as those with similar spatiotemporal demands, but struggles with platoon dispersion along the extended corridors as well as zone-to-zone transitions. To overcome the above shortcomings, this article considers the combination of control space and time division and proposes a method to divide an urban arterial road into appropriate space-time zones. This division is then tested using a dynamic coordinated signal control model.

2. Spatial Division Method

The spatial subarea division described in this article refers to the division of urban arterial roads into subareas according to the traffic characteristics of road sections and intersections. Most of the existing studies considered intersection relevance to divide the road network into subareas [30, 31], and spatial division must first meet the requirements of inter-intersection relevance [32, 33]. The idea of this division method is that when adjacent intersections are highly correlated, the two adjacent intersections must be coordinated. However, when the traffic flow is high and an intersection is oversaturated, vehicles will not be able to progress, which will inevitably cause vehicles to stop and wait. Obviously, this method is not suitable for green wave coordinated control, which requires a relatively unrestricted flow of traffic. Therefore, a reasonable division of spatial subareas should be based on the minimum requirements of traffic flow to ensure relevance while not exceeding the maximum capacity of the adjacent intersection. It should be pointed out that the maximum traffic capacity of adjacent intersections is referred to the traffic carrying capacity after the implementation of green wave control, which is related to the green wave bandwidth. In this case, the spatial subarea division method should have upper and lower limits.

2.1. Upper Limit of Subarea Division Threshold. The physical quantity Q is defined as the traffic flow, S is the spatial distance, and R is the degree of correlation of the intersection. Using real-time traffic volumes as input, the maximum green wave capacity between adjacent intersections and the actual traffic flow is calculated as shown in (1) and (2):

$$\text{Cap}_{i,i+1}^{\max} = \frac{\text{BW}_{i,i+1} * \min\left(\text{LN}_i, \text{LN}_{i+1}\right) * 3600}{C * \text{ht}}, \quad (i = 1, 2, \ldots, N), \tag{1}$$

$$Q_{i,i+1} = Q_{\text{sm},i} + Q_{\text{sl},i} + Q_{\text{sr},i} - Q_{\text{sl},i+1} - Q_{\text{sr},i+1}, \tag{2}$$

where $\text{Cap}_{i,i+1}^{\max}$ is the maximum number of vehicles that pass without stopping in one cycle from intersection i to intersection $i+1$; $\text{BW}_{i,i+1}$ is the green wave bandwidth from intersection i to intersection $i+1$; LN_i refers to the number of straight lanes at intersection i; LN_{i+1} refers to the number of straight lanes at intersection $i+1$; N is the number of intersections within the control range; C is the common signal cycle; ht is the saturated headway of vehicles passing through the intersection. As shown in Figure 1, $Q_{i,i+1}$ is the number of vehicles leaving the intersection $i+1$ in the co-ordinated direction; $Q_{\text{sm},i}$ is the number of straight vehicles in the west entrance direction of intersection i; $Q_{\text{sl},i}$ is the number of left-turning vehicles in the north entrance direction of intersection i; $\Delta\delta = 0.6$ is the number of right-turning vehicles in the south entrance direction of intersection i; $Q_{\text{sl},i+1}$ is the number of left-turning vehicles in the north entrance direction of intersection $i+1$; and $Q_{\text{sr},i+1}$ is the number of right-turning vehicles in the south entrance direction of intersection $i+1$.

If $Q_{i,i+1} < \text{Cap}_{i,i+1}^{\max}$, then the actual flow does not exceed the green wave capacity, and the coordinated control is required; if $Q_{i,i+1} \geq \text{Cap}_{i,i+1}^{\max}$, then the actual flow has exceeded the green wave capacity, and the coordinated control is not required.

2.2. Lower Limit of Subarea Division Threshold.

According to the degree of correlation among intersections, there is objectively a merging threshold for adjacent intersections. Assuming that the threshold for correlation degree of intersection merging is R_{com}, this value can then be adjusted according to the actual traffic environment to calculate the correlation degree of adjacent intersections by comparing their sizes to divide the subareas [34], as shown in (3) and (4):

$$R_{i,i+1} = \frac{Q_{i,i+1}}{S_{i,i+1}^2}, \tag{3}$$

$$Q_{i,i+1} = Q_{i,i+1}^u + Q_{i,i+1}^d, \tag{4}$$

where $R_{i,i+1}$ is the degree of correlation between adjacent intersection i and intersection $i+1$; $Q_{i,i+1}$ is the traffic volume of the adjacent intersection; $Q_{i,i+1}^u$ is the upward traffic volume of the road segment; $Q_{i,i+1}^d$ is the downward traffic volume of the road segment; and $S_{i,j+1}$ is the length of the road section of the adjacent intersection.

$R_{i,i+1} \geq R_{\text{com}}$ indicates that the degree of correlation of adjacent intersections is greater than the merge threshold, and the coordinated control is required, whereas $R_{i,i+1} < R_{\text{com}}$ indicates that the degree of correlation of adjacent intersections is less than the merge threshold, and the coordinated control is not required. The value of the merging threshold R_{com} can be referred to the recommended values shown in Table 1 [34].

This study is a two-way coordination control optimization. Considering that the threshold is lower threshold for the division of spatial subareas, and the correlation corresponding to no coordination is taken as the lower threshold, it can be determined that $R_{\text{com}} = 0.386$.

2.3. Division Results.

After calculating threshold limits, the n intersections on the arterial road can be divided into j co-ordinated control subareas $Z = (z_1, z_2, \ldots, z_j)$ in space according to the upper and lower thresholds. The k_{j-1}th intersection is set as the dividing intersection of subarea z_{j-1} and subarea z_j, denoted as $s_{k(j-1)}$. The following results can then be obtained:

$$z_1 = \left(s_1, s_2, \ldots, s_{k(1)}\right), \tag{5}$$

$$z_2 = \left(s_{k(1)+1}, s_{k(1)+2}, \ldots, s_{k(2)}\right), \tag{6}$$

$$z_i = \left(s_{k(i-1)+1}, s_{k(i-1)+2}, \ldots, s_{k(i)}\right), \tag{7}$$

$$z_j = \left(s_{k(j-1)+1}, s_{k(j-1)+2}, \ldots, s_n\right). \tag{8}$$

If there is only one intersection in the subarea z_i, then $k(i) - k(i-1) = 1$.

3. Temporal Division Method

In the existing literature, temporal division is most often applied to single intersections [35, 36]. The multi-period division of coordinated control on arterials is different from the multi-period division of a single intersection. Most importantly, the arterial control schemes must consider the intersection phasing and traffic volumes at multiple intersections, which is more complicated than the multi-period division method of a single intersection. In this section, a matrix is introduced to represent the traffic flow sequences of multiple intersections and multiple periods. The optimal division result can then be obtained by applying clustering approaches to the matrix.

3.1. Determination of the Best Clustering Method.

For any spatial coordination subzone $z_i = (s_{k(i-1)+1}, s_{k(i-1)+2}, \ldots, s_{k(i)})$, there are $N = k(i) - k(i-1)$ intersections in the space. The discussion takes a spatial coordination subarea as the time division unit, takes the traffic flow data $\mathbf{Q_t} = (q_1, q_2, \ldots, q_N)$ of each intersection in the time period t, and collects T samples in 24 hours a day. It is noted that $\mathbf{Q_t}$ refers to the traffic volume of the entire intersection at different intersections, which is different from $Q_{i,i+1}$ introduced in Section 2. The traffic sequences generated by a spatial coordination subarea 24 hours a day can be expressed as:

$$\mathbf{X} = \left(\mathbf{Q_1^T}, \mathbf{Q_2^T}, \ldots, \mathbf{Q_t^T}, \ldots, \mathbf{Q_T^T}\right), \tag{9}$$

where $\mathbf{X}$ is a sample matrix, which represents the data samples collected T times at N intersections in a spatial
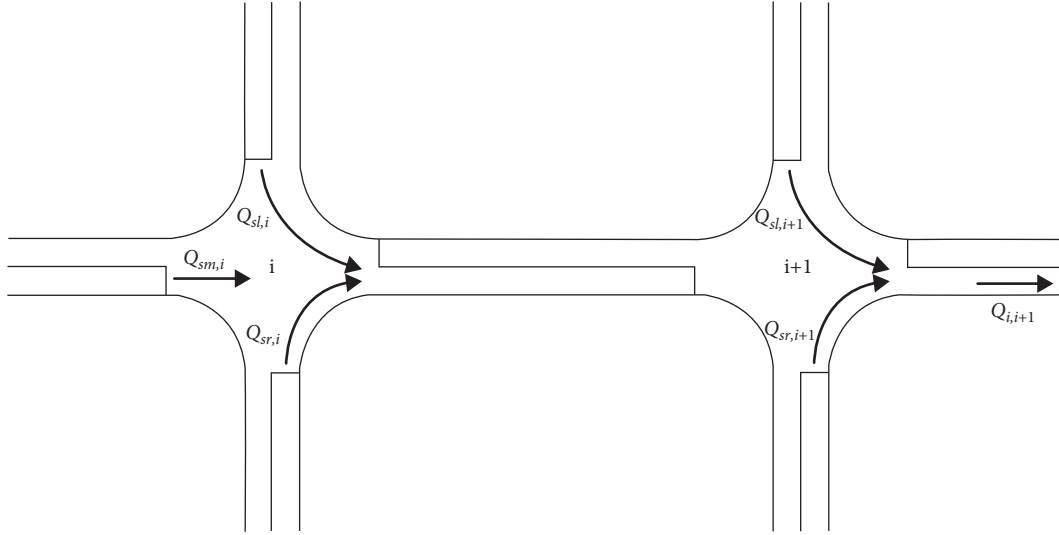
FIGURE 1: Schematic diagram of the traffic flow distribution at adjacent intersections.

TABLE 1: Intersection merge threshold recommendations.

Intersection correlation	Must coordinate	Can be coordinated	No coordination required
One-way traffic	≥ 19.3	< 19.3 and > 0.386	≤ 0.386
Two-way traffic	≥ 9.65	< 9.65 and > 0.193	≤ 0.193

coordination subarea. $\mathbf{Q_t}$ is a vector consisting of N intersection traffic data in time period t—its expansion can be expressed as:

$$\mathbf{X} = \begin{bmatrix} q_{11} & q_{12} & \cdots & q_{1T} \\ q_{21} & q_{22} & \cdots & q_{2T} \\ \cdots & \cdots & q_{ij} & \cdots \\ q_{N1} & q_{N2} & \cdots & q_{NT} \end{bmatrix}. \tag{10}$$

According to the definition of ordered clustering, assuming that there are $j - i + 1$ data samples included in the classification $\mathbf{C}$, then $\mathbf{C}$ can be expressed as follows:

$$\mathbf{C} = \left(\mathbf{Q_i}, \mathbf{Q_{i+1}}, \ldots, \mathbf{Q_j} \right), \quad (1 \leq i \leq j \leq T). \tag{11}$$

The ordered clustering algorithm groups the flow sequences with similar distributions and continuousness into one class, and each class corresponds to a control period. When describing the data difference of the partition class, the similarity of the data in the partition class is defined as the within-class distance $D(i, j)$, which can be calculated as follows:

$$D(i, j) = \left\| \mathbf{Q_t} - E_C \right\|, \quad t = (i, i + 1, \ldots, j), \tag{12}$$

where $D(i, j)$ is the within-class distance difference of the division class $\mathbf{C}$, that is, the degree of dispersion of the flow data from the ith time to the jth time, $\mathbf{Q_t}$ is the flow value corresponding to the tth time, and E_C is the division class $\mathbf{C}$.

If the T data in sequence $\mathbf{X}$ are divided into k partition classes and i_t is defined as the partition point of the partition class, then multiple partition points are denoted as $i_t = (i_1, i_2, \ldots, i_k)$ and satisfy $1 = i_1 < i_2 < \cdots < i_k < T$. (13) can be expressed as the partition result:

$$\{i_1, i_1 + 1, \ldots, i_2 - 1\}\{i_2, i_2 + 1, \ldots, i_3 - 1\} \cdots \{i_k, i_k + 1, \ldots, T\}. \tag{13}$$

For a traffic sequence with a limited number of samples, the division method has limited effectiveness. When this occurs, other available partitioning methods can be compared to determine the best approach. Then, it is necessary to evaluate the relatively accurate time division results in limited traffic data, which can solve this problem by using the idea of risk decision-making. In other words, by constructing the risk function, the division result corresponding to the minimum risk value is obtained, which is the minimum system loss. Here, $g(T, k)$ is defined as the objective function of a given partitioning method. In other words, the solution of $g(T, k)$ refers to the positions of k-1 division boundaries (i.e., the division result). Then the sum of the mathematical expectations of the intraclass distances of each class is taken, which means that the data difference in each class is the smallest, and the risk is considered to be the smallest here, which is the corresponding optimal division result. Therefore, if it has the smallest partitioning loss, it is selected as the most preferred method. The design risk function is shown in Equation (14):

$$R(T, k) = E_k [L(k, g(T, k))]$$
$$= \underset{t \in \Theta}{E} [\mathbf{D}(\mathbf{i_t}, \mathbf{i_{t+1}} - \mathbf{1})], \quad \Theta = (1, 2, \ldots, k). \tag{14}$$

$$L[g(T, k)] = \mathbf{D}(\mathbf{i_t}, \mathbf{i_{t+1}} - \mathbf{1}) = \begin{bmatrix} D(i_1, i_2 - 1) \\ D(i_2, i_3 - 1) \\ \vdots \\ D(i_k, T) \end{bmatrix}. \tag{15}$$

In this way, the determination of the best division method is actually transformed into a function minimization problem, that is the best division method $G(T, k)$ can be obtained by finding the $g(T, k)$ corresponding to the minimum value of the decision function $R(T, k)$, as calculated in the following equation:

$$G(T, k) = \arg \underset{t \in (1,2,\ldots,k)}{\min} R(T, k) = \arg \min \{E [\mathbf{D}(\mathbf{i_t}, \mathbf{i_{t+1}} - \mathbf{1})]\}. \tag{16}$$

$G(T, k)$ is solved on the premise that the value of k is known. Therefore, before obtaining $G(T, k)$, an optimal cluster number k is needed.

3.2. Determination of the Optimal Cluster Number.

To simplify the problem of finding the optimal cluster number, suppose that all possible results of the division of sample $\mathbf{X}$ are P, denoted as:

$$P = \left\{ \{x_1, x_2, \ldots, x_k\} | \mathbf{X} = \underset{h=1}{\overset{k}{\cup}} x_h, x_m \cap x_l = \varnothing, (m \neq l) \right\}. \tag{17}$$

The clustering performance is then evaluated. When the number of clusters is k, an abstract function is used here to explain the solution method. The time division criterion function is defined as $f_k(P) = f_k(\{x_1, x_2, \ldots, x_k\})$.. The problem of solving the optimal number of clusters is transformed into the solution of the combination problem of solving function $f_k(P)$, as shown in the following equation:

$$k_{\text{best}} = \arg \underset{k \in (2,3,\ldots,n)}{\min} f_k(\{x_1, x_2, \ldots, x_k\}), \tag{18}$$

where $\mathbf{X} = \cup_{h=1}^{k} x_h, x_m \cap x_l = \varnothing, (m \neq l), k \in (2, 3, \ldots, n)$..

The solution for the minimum value of f is a nonlinear maximum value problem. An improved simulated annealing method is used to solve the problem. The specific steps of the solution are as follows:

(i) Step 1: Randomly generate the initial k value and then calculate the criterion function $f_k(P)$, where $k \in [2, \sqrt{T}]$ and $K \in N^+$.

(ii) Step 2: The calculation produces a new value of k, which is recorded as k^*, and the current value of the criterion function $f_k(p)$ is calculated again.

(iii) Step 3: Obtain Δf_k, which is calculated by $\Delta f_k = f_k(k^*) - f_k(k)$.

(iv) Step 4: Determine whether Δf_k is less than or equal to 0. If yes, it is considered that k^* is better than k, and $k = k^*$, $f_k(k) = f_k(k^*)$ is executed at this time; if not, it is considered that k^* is not superior to k, but k^* is accepted with probability P_a, and $M = \gamma * M$ is executed at this time, where $r \in (0, 1)$ is related to the fluctuation degree of the traffic sequence.

$$P_a = \exp \left[\frac{-\Delta f_k}{M} \right]. \tag{19}$$

(v) Step 5: Determine whether the threshold number of iterations is reached; if yes, go to step 6; if not, go back to step 2.

(vi) Step 6: Determine whether the value of M at this time meets $M \leq \varepsilon$; if yes, output the value of k at this time, and the operation ends; if not, return to step 2 after executing $M = \alpha * M$; where ε is the calculation accuracy, and α meets $\alpha > \gamma$ and $\alpha \in (0.1)$.

The time division method of a space coordination subarea is described in Section 3. Similarly, the time division results of all the space coordination subareas of the arterial road can be obtained. It can be seen that the space coordination subareas are independent of each other, and they are not coordinated. The dynamic coordination control method is explained in Section 4.

4. Dynamic Coordinated Control Model

4.1. Model Framework.

The time and space of an urban arterial road are denoted as $\text{ST}(s_n, T)$. Taking the ordinate as the space and the abscissa as the time, an intuitive expression of the result of space division and time division can be represented in the Cartesian coordinate system (Figure 2).

In the space-time diagrams (Figure 2), the horizontal and vertical lines are the dividing lines of the space (coordination) and time (coordination) subareas, denoted as HL_i and VL_i, respectively. The enclosed space-time is the space-time (coordination) subarea, denoted as $z[s(i), t(j)]$. Among them, the positions of the horizontal and vertical lines are determined by the space and time division methods, respectively. The space-time effects generated by vehicles moving on urban arterial roads can be correspondingly distributed in the space-time diagram (Figure 2). Each space-time (coordination) subarea can be regarded as an independent system. When the traffic demand changes significantly across HL_i and VL_i, it will affect the whole stability of the transportation system. Therefore, the dynamic coordinated control of each space-time subarea is required. It is conceivable that if the time dimension is not considered and only the spatial partition is used, when the vehicle crosses the HL_i, a control plan is required inside each spatial coordination subarea, and a control plan is also required outside the adjacent spatial subarea. Instead, if the spatial dimension is not considered and only the time partition is taken, when the vehicle crosses the VL_i, the traffic
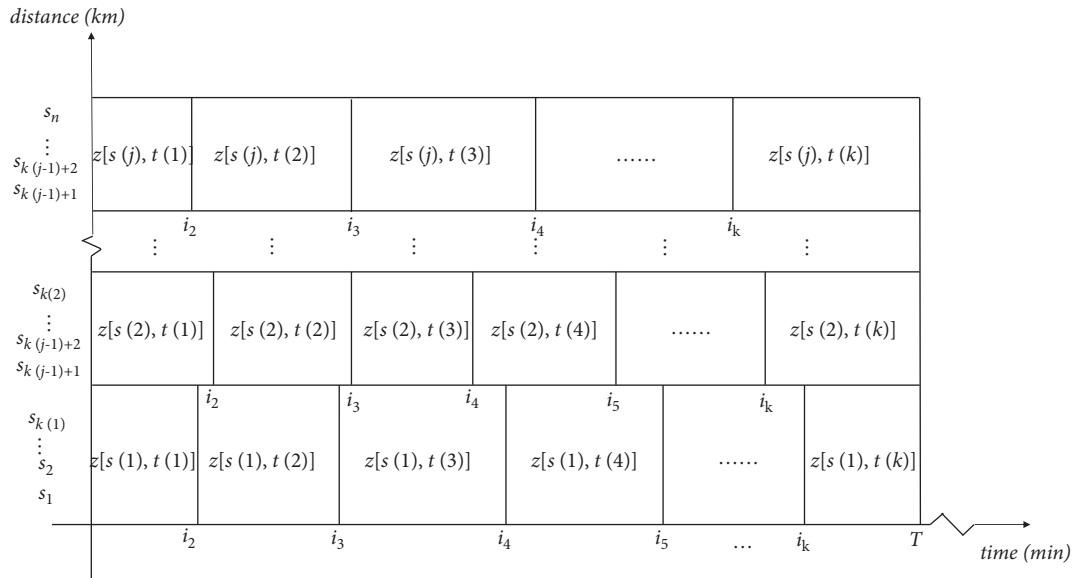
(a)
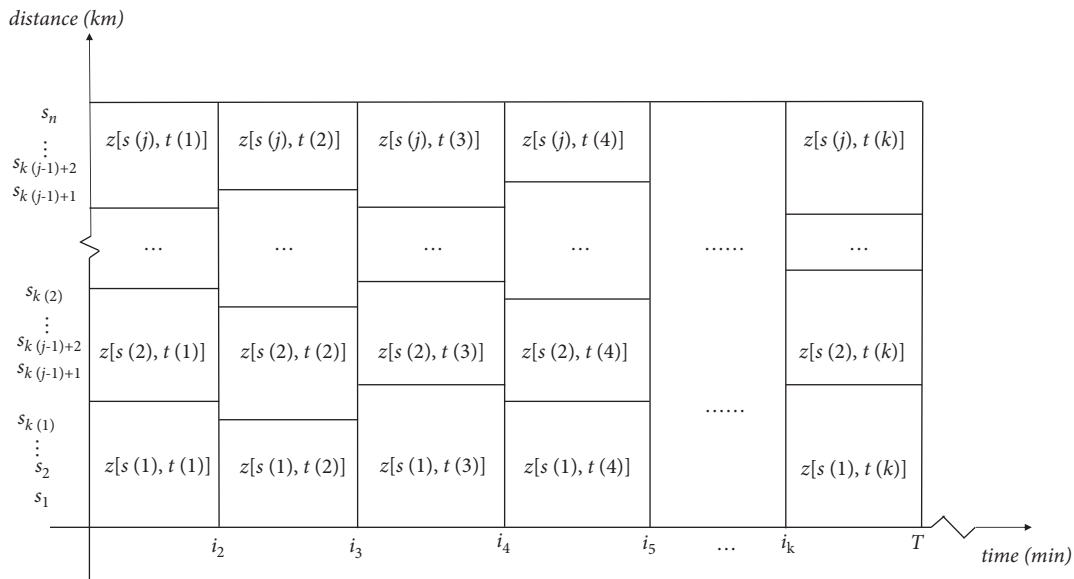
(b)

FIGURE 2: Schematic diagram of the division of time-space subareas and their coordination. (a) Perspective of time. (b) Perspective of space.

flow cannot quickly adapt to the new subarea plan, which can lead to traffic congestion. In this case, it is necessary to set a buffer time to overstep. The next section will elaborate on the specific coordinated control method.

4.2. Control Method

4.2.1. Internal Coordinated Control Method of Spatial Subareas. After dividing the spatial coordination subarea, the first thing to establish is that the spatial subarea is an independent system, and that its internal intersections are coordinated. In this study, a simple MAXBAND model is used to coordinate the internal intersections of the spatial subareas. Discussion on the specific timing plan method

development is omitted, but can be found in the literature [37].

4.2.2. Coordination Method of the Adjacent Space Coordination Subarea. This section discusses the coordinated control of the adjacent space coordination subarea [38, 39]. Assuming that at time zero, the relative phase between the last intersection in the upstream subarea and the first intersection in the downstream subarea, the difference is φ. Table 2 lists the definitions of model parameters and decision variables.

Under the above assumptions, the temporal and spatial distribution of traffic flow in adjacent subareas is shown in Figure 3. The detailed analysis is as follows:

TABLE 2: Symbolic definition of decision variables and constant.

| Type	Symbol	Definition
Constant	K	The least common multiple of the common periods T_1 and T_2 of the upstream subarea and the downstream subarea
	m	The cycle lengths of the first intersection in the downstream subarea within the least common multiple of time K
	n	The cycle lengths of the last intersection in the upstream subarea within the least common multiple of time K;
Decision variables	T_1	The length of the common cycle of the upstream subarea;
	T_2	The length of the common cycle of the downstream subarea;
	g_d	The green phase time for the coordinated direction of the first intersection in the downstream subarea;
	g_u	The coordinated direction green time of the last intersection in the upstream subarea;
	r_u	The red phase time for the coordinated direction of the last intersection in the upstream subarea;
	r_d	The red phase time for the coordinated direction of the first intersection in the downstream subarea;
	φ	The phase difference between the last intersection in the upstream subarea and the first intersection in the downstream subarea at time zero;
	t_u	The travel time from the last intersection in the upstream subarea to the first intersection in the downstream subarea;
	t_d	The travel time from the first intersection in the downstream subarea to the last intersection in the upstream subarea;
	$\varphi_{\max}$	The maximum phase difference between the last intersection in the upstream subarea and the first intersection in the downstream subarea at time zero, $\varphi_{\max} = \min(T_1, T_2)$;
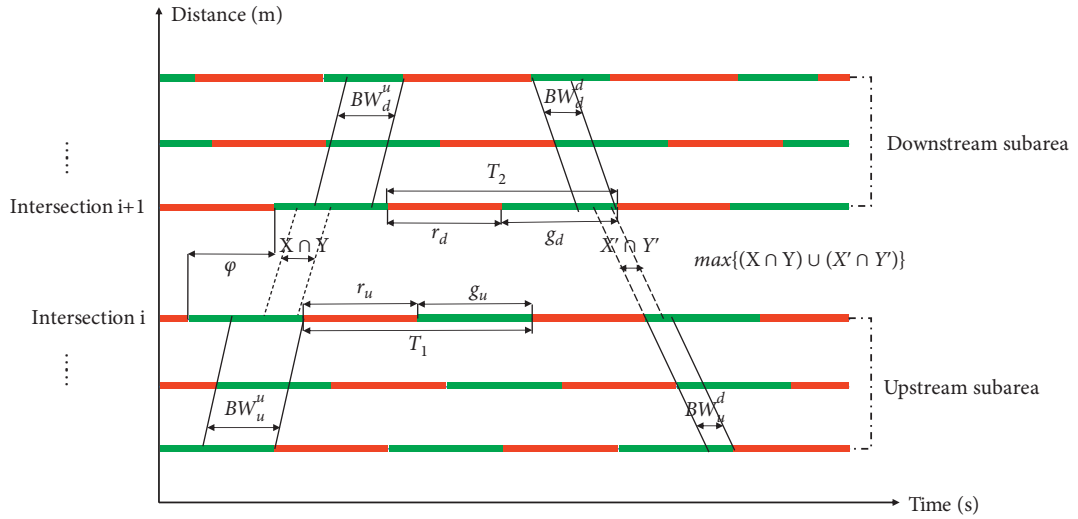
FIGURE 3: Schematic diagram of the coordination model of adjacent space subareas.

(i) Analysis 1: The time interval for a vehicle from intersection i to intersection $i+1$ can be expressed as follows:

$$\begin{cases} x_1 = (t_u, t_u + g_u), \\ x_2 = (t_u + T_1, t_u + g_u + T_1), \\ x_3 = (t_u + 2T_1, t_u + g_u + 2T_1), \\ \vdots \\ x_n = (t_u + nT_1 - T_1, t_u + g_u + nT_1 - T_1). \end{cases} \tag{20}$$

Then, in time $[0, K]$, the set of arrival time intervals from intersection i to intersection $i+1$ can be expressed as:

$$X = (x_1, x_2, x_3, \ldots, x_n). \tag{21}$$

(ii) Analysis 2: The green phase time interval of intersection $i+1$ is expressed as follows:

$$\begin{cases} y_1 = (\varphi, \varphi + g_d), \\ y_2 = (\varphi + T_2, \varphi + g_d + T_2), \\ y_3 = (\varphi + 2T_2, \varphi + g_d + 2T_1), \\ \vdots \\ y_m = (\varphi + mT_2 - T_2, \varphi + g_d + mT_2 - T_2). \end{cases} \tag{22}$$

Then, in time $[0, K]$, the set of green phase time intervals at intersection $i+1$ is expressed as:

$$Y = (y_1, y_2, y_3, \ldots, y_n). \tag{23}$$

(iii) Analysis 3: In the same way, the time interval for the opposite direction vehicle from intersection $i+1$ to

intersection i and the green phase time interval for intersection i can be obtained, as shown below:

$$\begin{cases} x_1' = (\varphi + t_d, \varphi + t_d + g_d), \\ x_2' = (\varphi + t_d + T_2, \varphi + t_d + g_d + T_2), \\ x_3' = (\varphi + t_d + 2T_2, \varphi + t_d + g_d + 2T_2), \\ \vdots \\ x_m' = (\varphi + t_d + mT_2 - T_2, \varphi + t_d + g_d + mT_2 - T_2). \end{cases}$$
(24)

Then, in time $[0, K]$, the set of time intervals for vehicles from intersection $i + 1$ to intersection i can be expressed as:

$$X' = (x_1', x_2', x_3', \ldots, x_m').$$
(25)

(iv) Analysis 4: The green phase time interval of intersection i is expressed as follows:

$$\begin{cases} y_1' = (0, g_u), \\ y_2' = (T_1, g_u + T_1), \\ y_3' = (2T_1, g_u + 2T_1), \\ \vdots \\ y_n' = (nT_1 - T_1, g_u + nT_1 - T_1). \end{cases}$$
(26)

Then, in time $[0, K]$, the set of green phase time intervals for intersection i can be expressed as:

$$Y' = (y_1', y_2', y_3', \ldots, y_n').$$
(27)

Through the above four analysis steps, the problem of the best coordinated phase difference ϕ_{best} between two adjacent subareas is transformed into the following maximization problem.

$$\text{Maximize } Z = \text{card}((X \cap Y) \cup (X' \cap Y')), \forall n \in N^+, m \in N^+.$$
(28)

Subject to:

$$\begin{cases} 0 \le \varphi \le \varphi_{max}, \\ \varphi_{max} = \min(T_1, T_2), \\ T_1 \ne T_2, \\ \varphi \in N^+, \\ Eq(1), (2), (3), (4), \end{cases}$$
(29)

Then,

$$\varphi_{best} = \arg \max |(X \cap Y) \cup (X' \cap Y')|.$$
(30)

From the above analysis, there is only one unknown variable φ in the set of X, Y, X', and Y'. Since the value range of φ is limited, the solution of the maximum value of $|(X \cap Y) \cup (X' \cap Y')|$ can be optimized by enumeration method. $|(X \cap Y) \cup (X' \cap Y')|$ denotes that the overlap between the vehicle arrival time interval and the green light time interval is maximized under the condition that the

vehicle is traveling at the desired speed. It can be equivalent to the relative movement of intersection i and intersection $i + 1$ shown in Figure 2 to determine the optimal φ_{best} of the system. The solution steps are as follows, where IV and IV_{max} are assignment variables.

Step 1: Input $\varphi_{max}, T_1, T_2, m, n$ and signal timing related parameters, initialize: $\varphi = 0, \text{IV}_{max} = 0$;

Step2: Calculate the value of IV at this time, $\text{IV} = \{\varphi | (|(X \cap Y) \cup (X' \cap Y')|)\}$;

Step 3: Determine whether $\text{IV} > \text{IV}_{max}$ is satisfied; if yes, go to step 4; if not, go to step 5;

Step 4: Update the value of IV_{max}, perform $\text{IV}_{max} = \text{IV}$;

Step 5: Update the value of φ, perform $\varphi = \varphi + 1$;

Step 6: Determine whether $\varphi > \varphi_{max}$ is satisfied; if yes, go to step 7; if not, go to step 2;

Step 7: Output the φ value corresponding to IV_{max}, which is φ_{best}.

4.3. Dynamic Coordination Control Process. From the above sections, the division of spatial coordination subareas can overcome the control problems caused by the spatial traffic difference at different intersections of long urban arterials, and the division of time coordination subareas can overcome the control obstacles caused by the difference in temporal traffic distribution. At the same time, there is also an inherent relationship between the two divisions. By dividing the space coordination subareas, the control problems caused by the difference in traffic distribution in the time dimension can be alleviated to a certain extent. Similarly, the time coordination subareas can also be divided into a certain degree. However, it is clear that the two control methods are applicable to different traffic scenarios and have different limitations. They cannot be applied to the more general traffic environment. Therefore, it is necessary to combine the two approaches for implementing an effective dynamic traffic control. The combined dynamic control process is as follows:

(i) Process 1: Use fixed-time control to make the system run for a equal to several system cycles C_S, and at the same time collect real-time flow across each time and space distribution in all cycle control systems. The system cycles can be calculated as follows:

$$C_S = [\max\{c_1, c_2, \ldots c_i\}, \min\{c_1, c_2, \ldots, c_i\}],$$
(31)

where c_i represents the common period of the space coordination subarea i;

(ii) Process 2: Take the data of the current system cycle as the basis and combine the data of the previous $b - 1$ system cycles to obtain the new b system cycle data as the input data of the controller. According to the data of b system cycles, update the current internal signal timing plan of each spatial subarea.

(iii) Process 3: Determine whether the space coordination subarea meets the update frequency f_{space}

requirement. If yes, go to process 4; if not, go back to process 2.

(iv) Process 4: Update HL_i according to the method shown in Equations (1)–(8). At this time, the system needs to set a minimum period transition period so that the vehicle can adapt to the new timing scheme. At the same time, the controller calculates the coordination plan of each adjacent space coordination subareas as well as the coordination plans within the space coordination subarea of the current system cycle.

(v) Process 5: The controller publishes the newly calculated signal control plan, which is displayed on the signal heads in all directions at the intersection through wired connections.

(vi) Process 6: Determine whether the boundary of the coordination subarea at the current time is reached. If yes, go to process 7; if not, go back to process 2.

(vii) Process 7: Judge whether the requirement of the update frequency f_{time} of the time coordination subarea is met. If yes, proceed to process 8; if not, go back to process 2.

(viii) Process 8: Update VL_i according to the method shown in Equations (9)–(19), and then return to process 2.

Among the above eight processes, a and b can be adjusted according to the control accuracy; f_{space} and f_{time} are suitable for different traffic environments and should be determined according to the specific traffic characteristics of the controlled arterial line, and further research is needed to determine the best f_{space} and f_{time}. To further illustrate how the dynamic coordinated control process is integrated into the overall coordinated control framework, the main process of the dynamic coordinated control is shown in Figure 4.

5. Experimental Verification

5.1. Experimental Design

5.1.1. Experiment Overview.
To evaluate the performance of the proposed control model in the actual traffic environment, a section of Zhongshan North Road in Guilin, Guangxi was selected as a case study. As shown in Figure 5, Zhongshan Road is one of the most important traffic arteries in the old city of Guilin, running through the central city of Guilin. Spatial and temporal traffic demand on Zhongshan Road is both variable and unpredictable, making Zhongshan Road an ideal case study for verifying the models and methods proposed in this research.

A video monitor is installed in each direction of each intersection to collect traffic volumes and other measures of effectiveness in real time. Using PTV VISSIM to simulate the occurrence of real-time traffic conditions, the real-time traffic data collected by the monitor are stored in the database, so that the VISSIM can read it in real time and obtain the traffic data source. The lane distribution and background

timing of intersections along the north section of Zhongshan Road are shown in Table 3, and the corresponding letters are also assigned to each intersection.

5.1.2. Determination of the Parameters and Functions of the Control Model.
When dividing the time coordination subareas, the optimal number of time coordination subareas is determined. To rapidly generate the best number of divisions and improve algorithm speed, the criterion function f_k shown in (32) is selected in this study [38].

$$f_k(h) = -\frac{1}{h} \sum \mathrm{BWACR}(j.i), \tag{32}$$

where $\mathrm{BWACR}(j.i)$ represents the clustering validity index of the ith sample in the jth divided class, which is the ratio of the minimum cosine value of the interclass angle to the average cosine value of the intraclass angle. The initial value of M involved in the algorithm represents the initial annealing temperature; γ is the parameter that controls the number of inner cycles; α is the parameter that controls the number of outer cycles; and ε is the calculation accuracy of the algorithm. Their values in this study [39] are shown in Table 4.

In addition, the values of green wave control parameters and dynamic coordinated control parameters are determined in the subarea. Considering the speed of the green wave belt and the stability of the green waves in the subarea, the cycle and speed need to be restricted. The values of related parameters are shown in Table 5. In the dynamic coordinated control parameters, a represents the time to collect traffic data before the dynamic coordinated control; b represents the learning range of the signal controller. The larger the value, the more accurate the decision-making in the control area, but the longer time required for calculation. Elsewhere, f_{space} is the dynamic adjustment frequency of the space coordination subarea, f_{time} is the dynamic adjustment frequency of the time coordination subarea. The values of f_{space} and f_{time} theoretically have the optimal values and correspond to each control state. Their values in this simulation experiment are shown in Table 6 [40, 41].

5.2. Simulation Experiment

5.2.1. Experimental Data Input.
The microscopic traffic modeling software VISSIM developed by PTV Group is used for the simulation experiment. The input data of this experiment include real-time traffic flow data and corresponding signal timing plans. In the experiment, the input data are stored in the database as real-time flow data collected by on-site video monitor, and VISSIM is continuously called and read during the operation. At the same time, the signal control method proposed in this study is written into the VISSIM timing algorithm to generate a signal control scheme based on the flow data read from the database in real time. Figure 6 shows the actual traffic volumes between October 19, 2020 00:00:00 and October 20, 2020 23:59:59 in the north section of Zhongshan Road, Guilin.
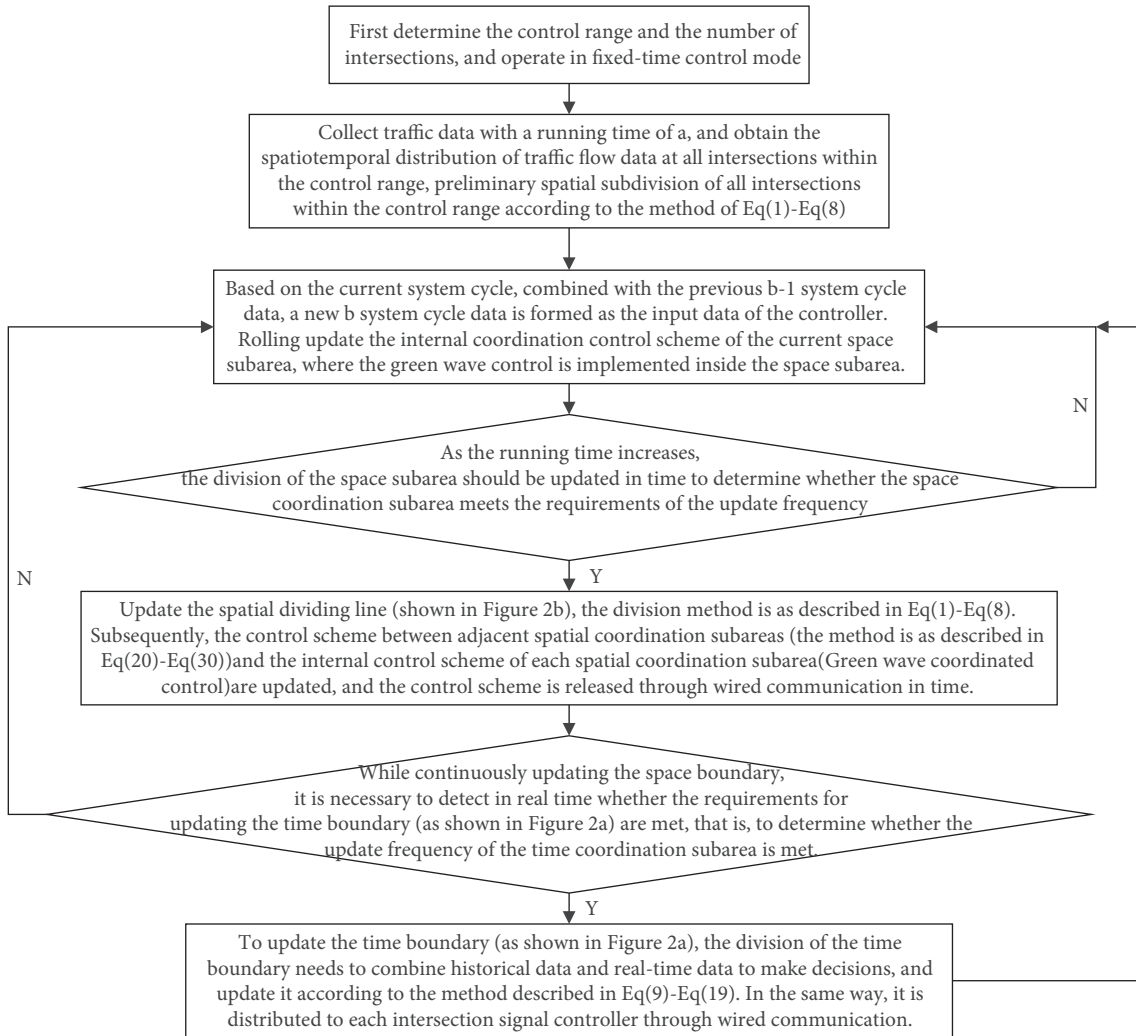
FIGURE 4: Flow chart of the dynamic coordination control.

FIGURE 5: Experimental location and equipment.

If the abscissa is the time and the ordinate is the actual intersection, a heat map of the temporal and spatial distribution of traffic flow can be obtained, as shown in Figure 6(c). In this subfigure, the darker color indicates

higher traffic volumes. The peak periods for each intersection of Zhongshan Road are observed at different times, while the traffic volume magnitudes are highly variable. Given these characteristics combined with the large

TABLE 3: Intersection lane distribution and background signal timing.

Intersection and corresponding letters	Lane distribution and number of lanes	Background signal timing
Fanghua Road and Zhongshan Road; A		
Xinjian Road and Zhongshan Road; B		
Beicang Road and Zhongshan Road; C		
Qunzhong Road and Zhongshan Road; D		
North Ring 2nd Road and Zhongshan Road; E		

TABLE 3: Continued.

Intersection and corresponding letters	Lane distribution and number of lanes	Background signal timing
Yushan Road and Zhongshan Road; F		
Ludi Road and Zhongshan Road; G		

TABLE 4: Parameter values of the simulated annealing method.

Parameter	M	γ	α	ε
Value	10	0.95	0.98	0.0001

TABLE 5: Value of the green wave coordinated control variable in the subarea.

Variable	$C_{\max\ (s)}$	$C_{\min\ (s)}$	$v_{\max(km/h)}$	$v_{\min(km/h)}$
Value	150	60	60	30

TABLE 6: Values of the dynamic coordination control parameters.

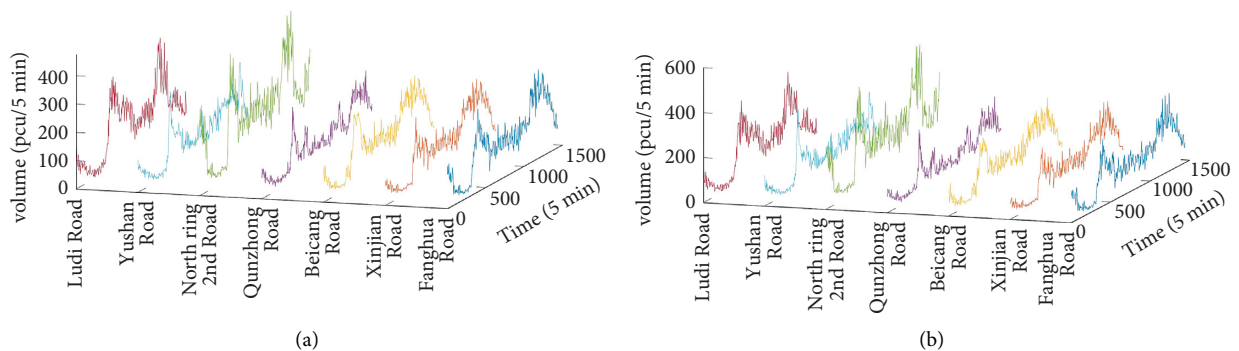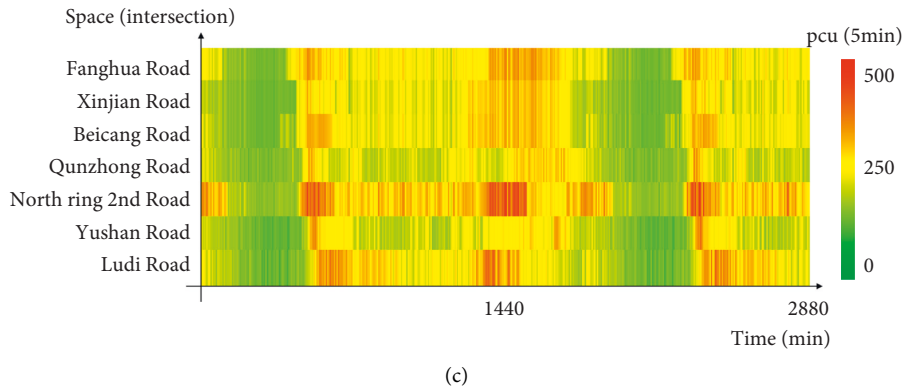| Parameter	a	b	f_{space}	f_{time}
Value	48 hours	$5C_S$	Every C_S	Every 24 hours

(a)

(b)

FIGURE 6: Continued.

(c)

FIGURE 6: The 48-hour traffic volume and heat map of each intersection. (a) Traffic volume trend on October 19. (b) Traffic volume trend on October 20. (c) Heat map of each intersection.
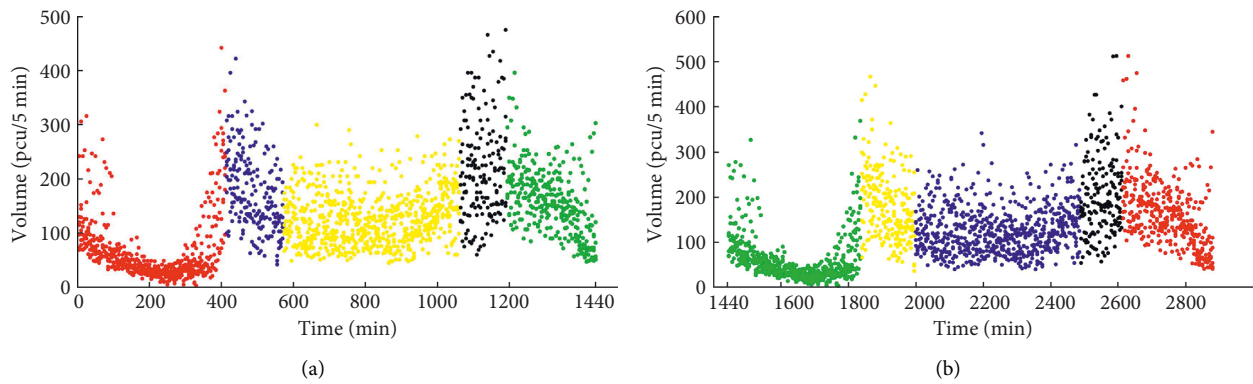

(a)

(b)

FIGURE 7: Temporal characteristics of the traffic flow clustering results.

TABLE 7: The 48-hour time-space division results of Zhongshan Road.

	Time division result	Space division result				
October 19, 2020	00:00–06:50	00:00–01:20 A/BCD/EF/G	01:20–05:15 A/BC/D/EFG	05:15–06:50 A/BCD/EFG		
	06:50–09:25	06:50–07:30 A/BCD/EFG	07:30–08:45 ABCD/EFG	08:45–09:25 ABCDEFG		
	09:25–17:05	09:25–11:35 A/BCD/EFG	11:35–12:50 ABCD/EFG	12:50–14:20 A/BCD/EFG	14:20–16:25 A/BCD/EF/G	16:25–17:05 A/BCD/EFG
	17:05–19:15	17:05–17:45 ABCD/EFG	17:45–18:40 ABCDEFG	18:40–19:15 ABCD/EFG		
	19:15–00:00	19:15–20:30 ABCD/EF/G	20:30–22:45 A/BCD/EFG	22:45–00:00 A/BCD/EFG		
October 20, 2020	00:00–06:35	00:00–01:05 A/BCD/EFG	01:05–05:25 A/BC/D/EF/G	05:25–06:35 A/BCD/EFG		
	06:35–09:15	06:35–07:35 A/BCD/EFG	07:35–09:15 ABCD/EFG			
	09:15–17:25	09:15–11:30 A/BCD/EFG	11:30–12:55 ABCD/EFG	12:55–14:15 A/BCD/EFG	14:15–16:45 A/BCD/EF/G	16:45–17:25 A/BCD/EFG
	17:25–19:30	17:25–18:15 ABCD/EFG	18:15–19:30 ABCDEFG			
	19:30–00:00	19:30–20:35 ABCD/EFG	20:35–22:40 A/BCD/EFG	22:40–00:00 A/BCD/EF/G		

distances between signals, the coordination along this arterial is difficult with a single control strategy, thus necessitating subdivided time and space strategies.

5.2.2. Experimental Scenario Setting. The existing studies on the coordinated control of multiple intersections can be divided into two categories: (a) The first category is about the
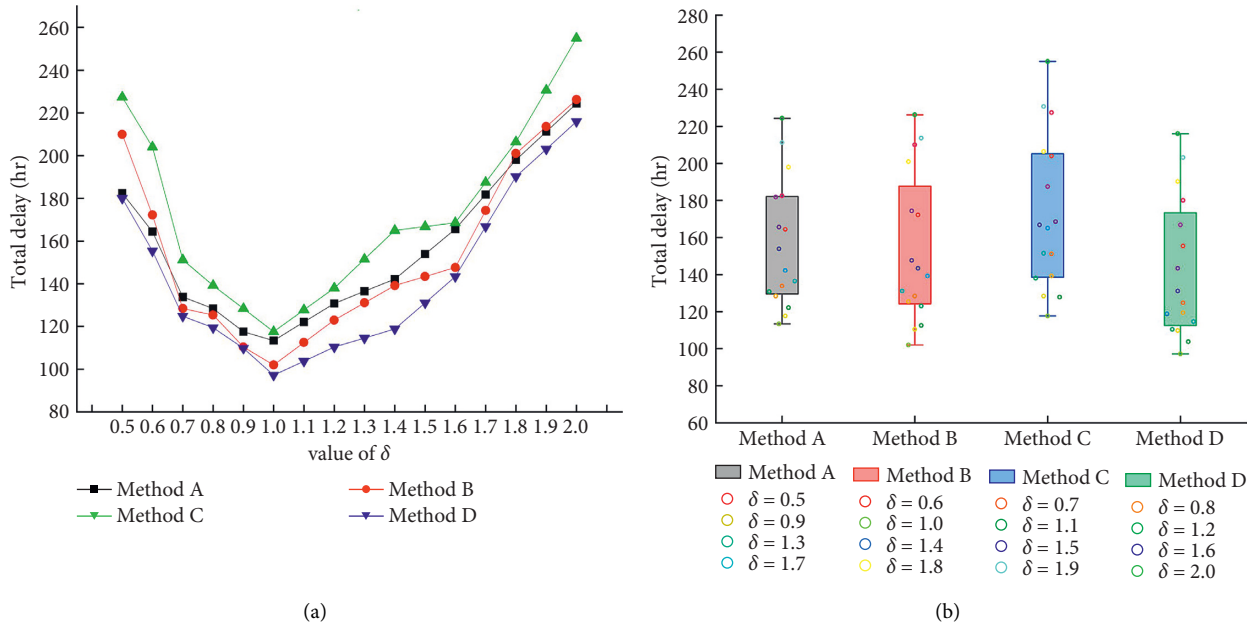
(a)

(b)

FIGURE 8: The total delay of the four control methods under different traffic environments.
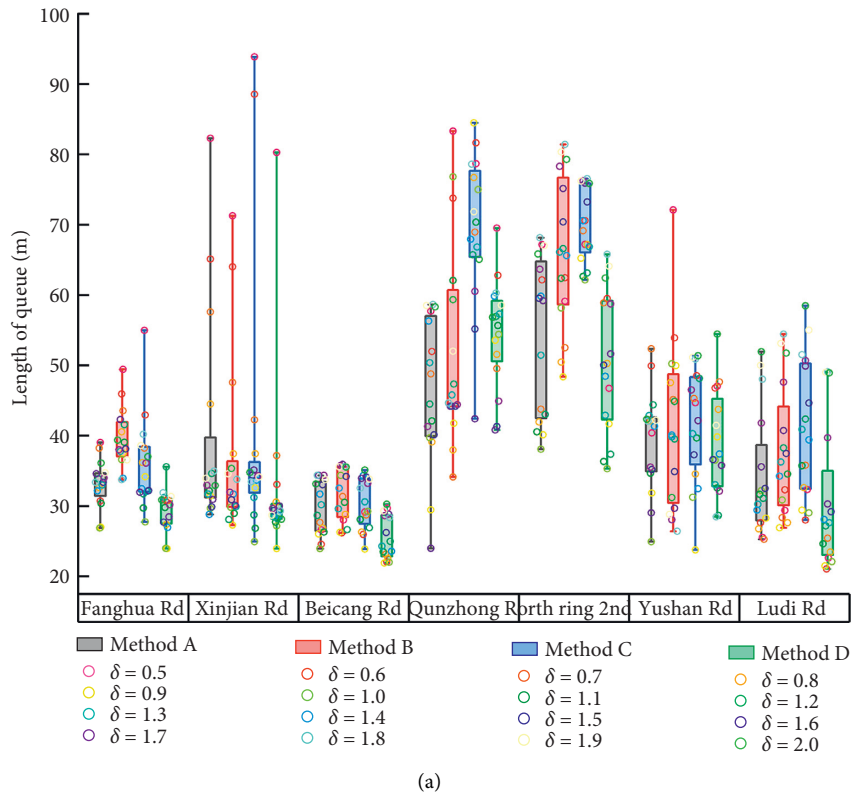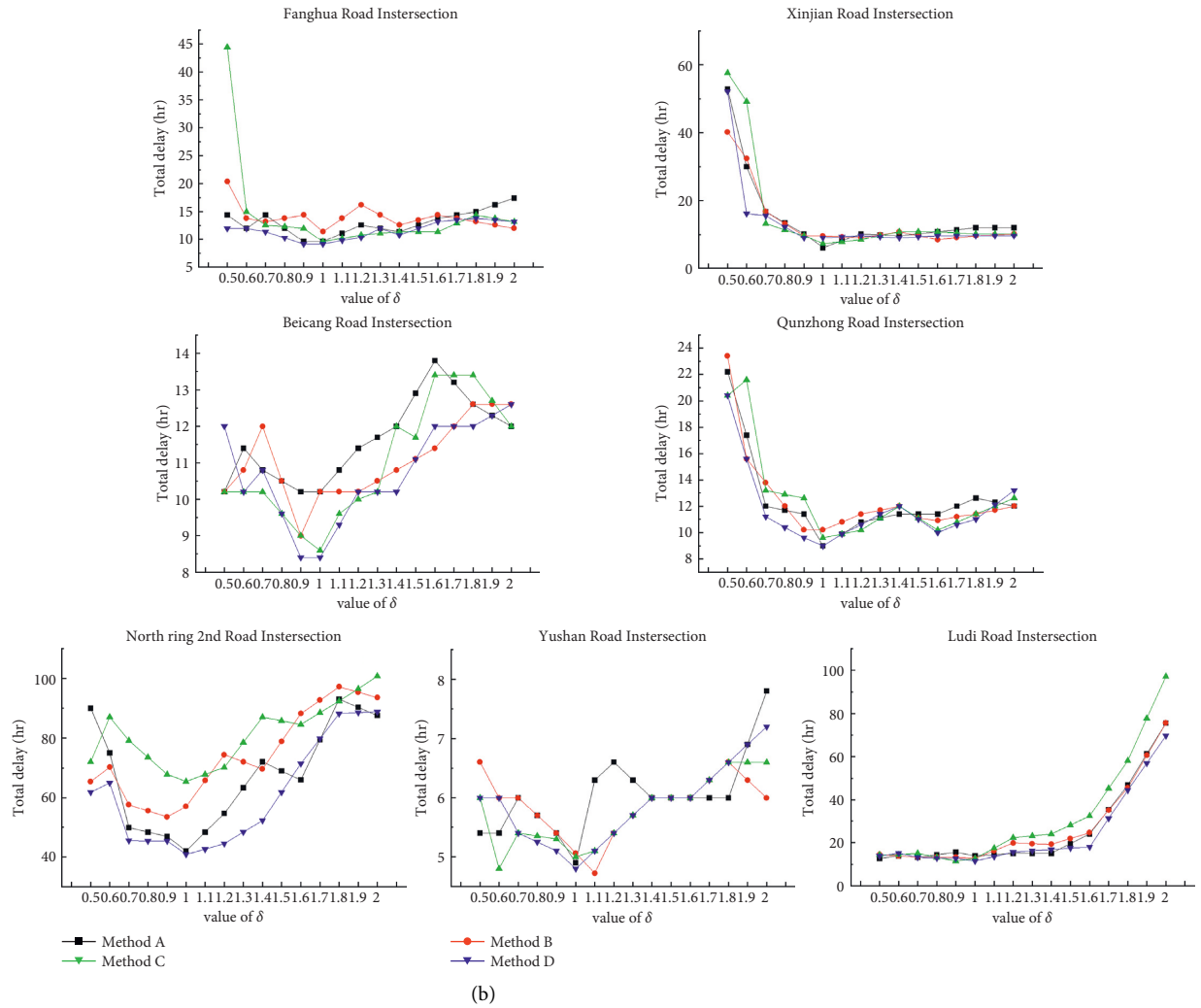

(a)

FIGURE 9: Continued.

FIGURE 9: Delays and queue length levels at various intersections under different control methods and different traffic environments.

dynamic division and optimization of the boundary of the control subarea in space; and (b) the second category is the subarea control of traffic flow in the time dimension through different clustering methods. To verify the control potential and performance of the control method proposed in this research in different traffic environments, four comparative control methods are set up in the experiment. They are control method A (only divide the space coordination subareas, the first category method), control method B (only divide the time coordination subarea, the second category method), control method C (ordinary green wave control, base case), and control method D (spatial-temporal division, the method proposed in this research). Under the premise of ensuring that the overall traffic volume remains unchanged, an unbalanced bidirectional traffic flow scenario was tested, with the directional flow ratio expressed as δ. The experiment consisted of 16 traffic environments with δ ranging from 0.5 to 2.0. Each scenario was tested against the four control methods separately.

5.2.3. Space-Time Division Results. Using the proposed method and the collected data, the results of the temporal

clustering are presented in Figure 7, while those of the spatial division methods are shown in Table 7. The letters ABC-DEFG correspond to the seven intersections of Zhongshan Road, and "/" represents the dividing line of the spatial subareas.

5.3. Experimental Data Analysis

5.3.1. Comparative Analysis of the Experimental Indicators. Since the simulation experiment does not change the phase length of the intersecting roads, the relative delay of the intersecting roads will not change, thereby allowing a direct comparison among all the four methods. The simulation experiment ran continuously for 48 hours of simulation time, and therefore the measured total delay times were relatively large. In order to facilitate direct comparison and analysis, the total delay was converted into an average total delay per hour. Figure 8 shows the delay for each control method across various flow balance ratios.

As shown in Figure 8, the performance of the proposed method varies across different traffic environments.
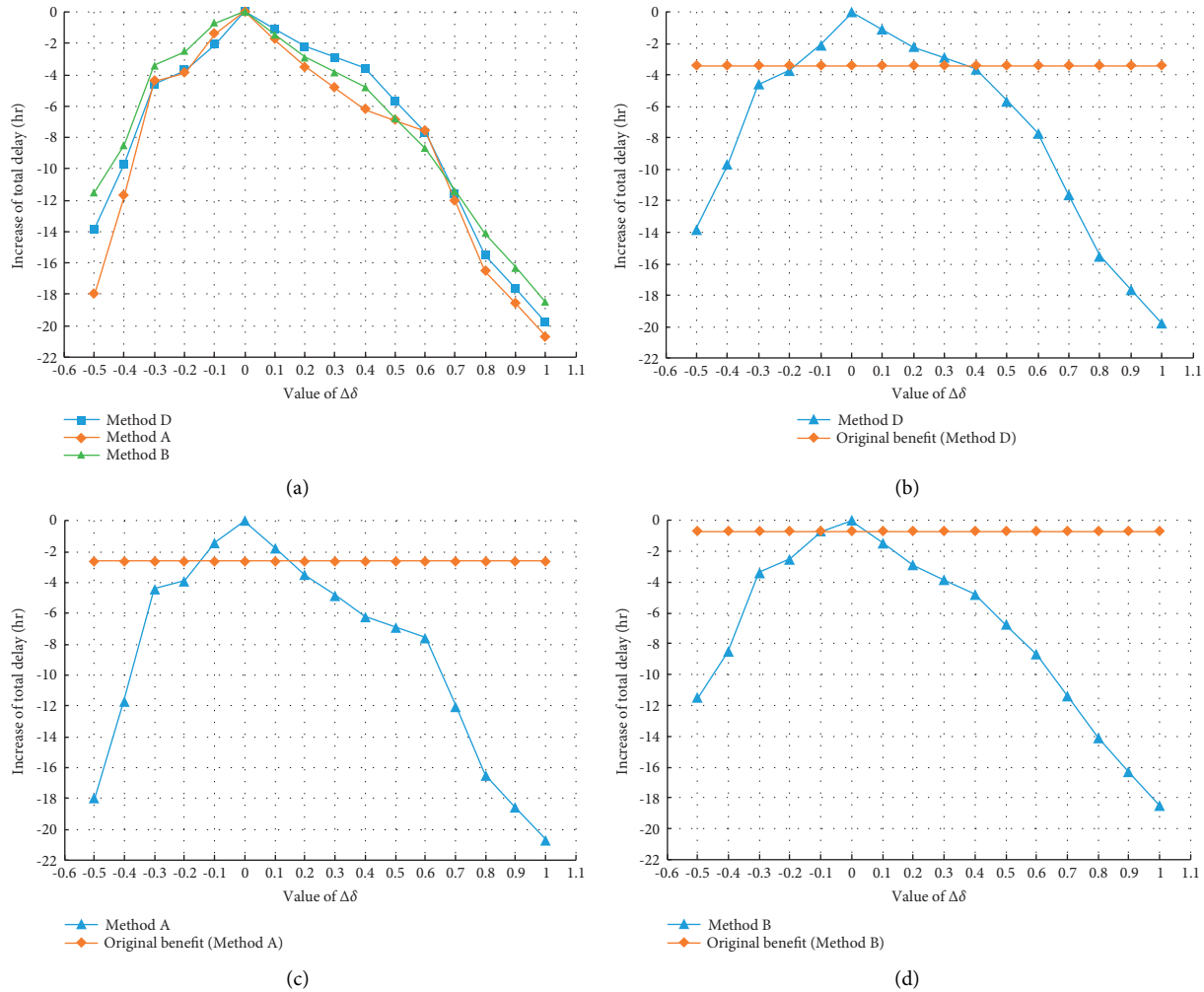
FIGURE 10: The control benefit change trend chart of each control method.

Obviously, it performs better than the existing control methods, and it shows the lowest delay under the conditions of different proportions of two-way traffic. The result also demonstrates that method A, method B, and method D exhibit less vehicle delay than method C, and method D produces the least vehicle delay. Method A and method B exhibit advantages in different traffic environments. When the two-way traffic volume tends to be balanced, method A is dominant; when the two-way traffic volume tends to be severely unbalanced, that is, in a severe tidal traffic environment, method B is dominant. For the average total delay of 1 hour for each control method and flow ratio, method C is the control group (Figure 8). It can also be seen from the table that the optimization of method D produces the lowest delays. The optimization of each control method under different values of δ produce different outcomes, which may be closely related to the road structure, intersection channelization, and lane division. The influence of these factors on subdivision and control delay remains an area for future research.

Although the division method is designed to optimize for delay, similar results were found for queue. Figure 9 displays the performance of the test algorithms on total delay and queue length of each intersection across all directional balance ratios.

The figure shows that the different inbound directions of T-shaped intersections have a greater impact on coordinated control and are also closely related to the traffic volume at the intersection. However, longitudinal observation can reveal that the control method D performs better, especially at North Ring 2nd Road Intersection with a large traffic volume, where the degree of optimization is the most obvious.

5.3.2. Sensitivity Analysis. The total delay of the coordination system is used as the optimization metric, and δ is adjusted to measure the sensitivity of each control method. To facilitate comparison, the total delay of each coordination system is transformed into an average total delay of 10 minutes, with method C used as the baseline comparison method against other methods. The original control benefit is the difference between the current method and method C at $\delta = 1.0\,(\Delta\delta = 0)$, and the control benefit change trend

chart is shown in Figure 10. It can be seen from (a) that the changes in the control benefits of the three control methods under different $\Delta\delta$ values are roughly the same. The results can be summarized as follows: when between $[-0.3, 0.6]$, the control benefits decrease gradually; when between $[-0.5, -0.3]$ and $[0.6, 1.0]$, the control benefits decline more rapidly. The inflection point is roughly at $\Delta\delta = -0.3$ and $\Delta\delta = 0.6$.

The control benefits are greatest when the two-way traffic volume is balanced, but in general, the two-way traffic volume is unbalanced. Therefore, we need to determine whether the range of the $\Delta\delta$ control benefits of each control method is acceptable. For example, as shown in (b), two broken lines have two intersection points. The $\Delta\delta$ corresponding to these two points are -0.181 and 0.372, which are recorded as $\Delta\delta_a(D) = -0.181$ and $\Delta\delta_b(D) = 0.372$. Similarly, as shown in (c) and (d), $\Delta\delta_a(A) = -0.148$ and $\Delta\delta_b(A) = 0.149$, $\Delta\delta_a(B) = -0.1$ and $\Delta\delta_b(B) = 0.048$. In (a), from the overall point of view, the broken line corresponding to the control method A is below the broken lines corresponding to the control methods B and D, indicating that the control method A is more sensitive than the control methods B and D. This suggests that the ability of control method A to resist traffic variation is weak. Furthermore, it can be seen from $\Delta\delta_b(D) - \Delta\delta_a(D) > \Delta\delta_b(B) - \Delta\delta_a(B) > \Delta\delta_b(A) - \Delta\delta_a(A)$ that the scope of application of the control method D is wider, implying that the control method D has a stronger anti-interference ability. In summary, the control method D is superior to the control methods A and B and has the advantages of weaker sensitivity and wider application range. This interpretation is supported by the broken line graph shown in Figure 8.

6. Conclusion

For long urban arterial roads operating under 24-hour signal control plans, the dynamic coordination method proposed in this article performs well under different traffic conditions. The proposed method can significantly reduce both control delay and queue length at intersections and has the advantages of strong resistance to shifts in traffic flow. When the two-way traffic imbalance coefficients are 0.5, 1.0, and 2.0, the corresponding delay optimization percentages are 26.33%, 20.99%, and 18.06%, respectively. However, this article does not consider the impact of pedestrian crossing and bus priority. The impact of these as well as other geometric factors is the focus of future research.

Data Availability

The data used to support the findings of this study are included within the article and are available from the corresponding author upon request.

Conflicts of Interest

The authors declare that they have no conflicts of interest.

Acknowledgments

References

[1] J. T. Morgan and J. D. C. Little, "Synchronizing traffic signals for maximal bandwidth," *Operations Research*, vol. 12, no. 6, pp. 896–912, 1964.

[2] J. D. C. Little, "The synchronization of traffic signals by mixed-integer linear programming," *Operations Research*, vol. 14, no. 4, pp. 568–594, 1966.

[3] J. Yan, P. Shao, Q. Chen, M. Zhang, Z. Li, and L. Wang, "A Study of Bidirectional Green Wave Control Based on Random Optimal Graphical Method," in *Proceedings of the 2018 IEEE 7th Data Driven Control and Learning Systems Conference (DDCLS)*, pp. 1180–1184, Enshi, China, May2018.

[4] K. Lu, J. Hu, J. Huang, D. Tian, and C. Zhang, "Optimisation model for network progression coordinated control under the signal design mode of split phasing," *IET Intelligent Transport Systems*, vol. 11, no. 8, pp. 459–466, 2017.

[5] X. Li, Z. Zhao, L. Liu, Y. Liu, and P. Li, "An optimization model of multi-intersection signal control for trunk road under collaborative information," *Journal of Control Science and Engineering*, 2017.

[6] C. Ma, W. Hao, A. Wang, and H. Zhao, "Developing a co-ordinated signal control system for urban ring road under the vehicle-infrastructure connected environment," *IEEE Access*, vol. 6, pp. 52471–52478, 2018.

[7] J. Tan, M. Zhang, H. Li, W. w. Guo, and L. Wang, "A Bi-directional Green Wave Band Method under Asymmetric Phase Sequence Mode Based on Mobile Navigation data," in *Proceedigs of the 2018 IEEE 7th Data Driven Control and Learning Systems Conference (DDCLS)*, pp. 1191–1196, IEEE, Enshi, China, May2018.

[8] N. H. Gartner, S. F. Assmann, and F. Lasaga, "MULTIBAND--a Variable-Bandwidth Arterial Progression scheme," *Transportation Research Record*, p. 1990, 1287.

[9] N. H. Gartner and C. Stamatiadis, "Arterial-based control of traffic flow in urban grid networks," *Mathematical and Computer Modelling*, vol. 35, no. 5-6, pp. 657–671, 2002.

[10] N. H. Gartner and C. Stamatiadis, "Progression optimization featuring arterial- and route-based priority signal networks," *Journal of Intelligent Transportation Systems*, vol. 8, no. 2, pp. 77–86, 2004.

[11] C. Stamatiadis and N. H. Gartner, "MULTIBAND-96: a Program for variable-bandwidth progression optimization of multiarterial traffic networks," *Transportation Research Record*, vol. 1554, no. 1, pp. 9–17, 1996.

[12] X. Yang, Y. Cheng, and G. L. Chang, "A multi-path progression model for synchronization of arterial traffic signals," *Transportation Research Part C: Emerging Technologies*, vol. 53, pp. 93–111, 2015.

[13] C. Zhang, Y. Xie, N. H. Gartner, C. Stamatiadis, and T. Arsava, "AM-Band: an Asymmetrical Multi-Band model for arterial traffic signal coordination," *Transportation Research Part C: Emerging Technologies*, vol. 58, pp. 515–531, 2015.

[14] S. Kim, A. Hajbabaie, B. M. Williams, and N. M. Rouphail, "Dynamic bandwidth analysis for coordinated arterial

streets," *Journal of Intelligent Transportation Systems*, vol. 20, no. 3, pp. 294–310, 2016.

[15] T. Arsava, Y. Xie, N. H. Gartner, and J. Mwakalonge, "Arterial Traffic Signal Coordination Utilizing Vehicular Traffic Origin-Destination information," in *Proceedings of the 17th International IEEE Conference on Intelligent Transportation Systems (ITSC)*, pp. 2132–2137, IEEE, Qingdao, China, October2014.

[16] T. Arsava, Y. Xie, and N. H. Gartner, "Arterial progression optimization using OD-BAND: case study and extensions," *Transportation Research Record*, vol. 2558, no. 1, pp. 1–10, 2016.

[17] Z. Tian, T. Urbanik, and C. Messer, *A System Partition Approach to Improve Signal Timing*, Transportation Research Board, Washington, D.C., CD-ROM, 2003.

[18] N. Geroliminis and C. F. Daganzo, "Existence of urban-scale macroscopic fundamental diagrams: some experimental findings," *Transportation Research Part B: Methodological*, vol. 42, no. 9, pp. 759–770, 2008.

[19] Y. Ji and N. Geroliminis, "On the spatial partitioning of urban transportation networks," *Transportation Research Part B: Methodological*, vol. 46, no. 10, pp. 1639–1656, 2012.

[20] T. A. Hauser and W. T. Scherer, "Data mining tools for real-time traffic signal decision support & maintenance[C]//2001 IEEE International Conference on Systems, Man and Cybernetics. e-Systems and e-Man for Cybernetics in Cyberspace (Cat. No. 01CH37236)," *IEEE*, vol. 3, pp. 1471–1477, 2001.

[21] N. T. Ratrout, "Subtractive clustering-based K-means technique for determining optimum time-of-day breakpoints," *Journal of Computing in Civil Engineering*, vol. 25, no. 5, pp. 380–387, 2011.

[22] L. L. Dai, Z. L. Sun, D. B. Liu, and Y. Li, "An Improved Method of Traffic Control Period Division for Intersection Based on Signal Cycle Calculation," *Applied Mechanics and Materials*, vol. 253, pp. 1731–1735, 2013.

[23] X. Lin, "A Road Network Traffic State Identification Method Based on Macroscopic Fundamental Diagram and Spectral Clustering and Support Vector machine," *Mathematical Problems in Engineering*, 2019.

[24] H. Lan and X. Wu, "Research on Key Technology of Signal Control Subarea Partition Based on Correlation Degree analysis," *Mathematical Problems in Engineering*, 2020.

[25] X. Song, W. Li, D. Ma, Y. Wu, and D. Ji, "An enhanced clustering-based method for determining time-of-day breakpoints through process optimization," *IEEE Access*, vol. 6, pp. 29241–29253, 2018.

[26] D. Ma, W. Li, X. Song, Y. Wang, and W. Zhang, "Time-of-day breakpoints optimisation through recursive time series partitioning," *IET Intelligent Transport Systems*, vol. 13, no. 4, pp. 683–692, 2019.

[27] D. Ma, J. Xiao, X. Song, X. Ma, and S. Jin, "A back-pressure-based model with fixed phase sequences for traffic signal optimization under oversaturated networks," *IEEE Transactions on Intelligent Transportation Systems*, vol. 22, no. 9, pp. 5577–5588, 2021.

[28] H. Ding, Y. Di, Z. Feng, W. Zhang, X. Zheng, and T. Yang, "A perimeter control method for a congested urban road network with dynamic and variable ranges," *Transportation Research Part B: Methodological*, vol. 155, pp. 160–187, 2022.

[29] X. Niu, J. Zhu, C. Q. Wu, and S Wang, "On a clustering-based mining approach for spatially and temporally integrated traffic sub-area division," *Engineering Applications of Artificial Intelligence*, vol. 96, Article ID 103932, 2020.

[30] Z. Zhou, S. Lin, and Y. Xi, "A fast network partition method for large-scale urban traffic networks," *Journal of Control Theory and Applications*, vol. 11, no. 3, pp. 359–366, 2013.

[31] Y. Bie, D. Wang, and X. Qu, "Modelling correlation degree between two adjacent signalised intersections for dynamic subarea partition," *IET Intelligent Transport Systems*, vol. 7, no. 1, pp. 28–35, 2013.

[32] Y. Gao, J. Zhao, Z. Qin, Y. Feng, Z. Yang, and B. Jia, "Traffic Speed Forecast in Adjacent Region between Highway and Urban Expressway: Based on MFD and GRU model," *Journal of Advanced Transportation*, 2020.

[33] Z. Wang, H. Ding, B. Li, L. Bao, and Z Yang, "An energy efficient routing protocol based on improved artificial bee colony algorithm for wireless sensor networks," *IEEE Access*, vol. 8, pp. 133577–133596, 2020.

[34] H. N. Yagoda, E. H. Principe, C. E. Vick, and B. Leonard, "Subdivision of signal systems into control areas," *Traffic Engineering Inst Traffic Engr*, vol. 43, no. 12, 1973.

[35] Z. Chen, X. Hou, and C. Yang, "Training resource allocation for user-centric base station cooperation networks," *IEEE Transactions on Vehicular Technology*, vol. 65, no. 4, pp. 2729–2735, 2016.

[36] B. Cesme and P. G. Furth, "Self-organizing traffic signals using secondary extension and dynamic coordination," *Transportation Research Part C: Emerging Technologies*, vol. 48, pp. 1–15, 2014.

[37] Y. Hanmin, L. Hao, and S. Qianting, "An Improved Semi-supervised K-Means Clustering algorithm," in *Proceedings of the 2016 IEEE Information Technology, Networking, Electronic and Automation Control Conference*, pp. 41–44, IEEE, Chongqing, China, May2016.

[38] M. Hasegawa, "Verification and rectification of the physical analogy of simulated annealing for the solution of the traveling salesman problem," *Physical Review*, vol. 83, no. 3, 2011.

[39] C. Ma and R. He, "Green wave traffic control system optimization based on adaptive genetic-artificial fish swarm algorithm," *Neural Computing & Applications*, vol. 31, no. 7, pp. 2073–2083, 2019.

[40] G. j Shen and Y. y Yang, "A dynamic signal coordination control method for urban arterial roads and its application," *Frontiers of Information Technology & Electronic Engineering*, vol. 17, no. 9, pp. 907–918, 2016.

[41] Y. Wang, X. Yang, H. Liang, and Y. d. Liu, "A Review of the Self-Adaptive Traffic Signal Control System Based on Future Traffic environment," *Journal of Advanced Transportation*, 2018.